

*Satellite Image-Based Time Series
Observations of Vegetation Response to
Hurricane Irma in the Lower Florida Keys*

**Jan Svejksky, Danielle E. Ogurcak,
Michael S. Ross & Alex Arkowitz**

Estuaries and Coasts

Journal of the Coastal and Estuarine
Research Federation

ISSN 1559-2723

Estuaries and Coasts

DOI 10.1007/s12237-020-00701-8



Your article is protected by copyright and all rights are held exclusively by Coastal and Estuarine Research Federation. This e-offprint is for personal use only and shall not be self-archived in electronic repositories. If you wish to self-archive your article, please use the accepted manuscript version for posting on your own website. You may further deposit the accepted manuscript version in any repository, provided it is only made publicly available 12 months after official publication or later and provided acknowledgement is given to the original source of publication and a link is inserted to the published article on Springer's website. The link must be accompanied by the following text: "The final publication is available at link.springer.com".



Satellite Image-Based Time Series Observations of Vegetation Response to Hurricane Irma in the Lower Florida Keys

Jan Svejkovsky¹ · Danielle E. Ogurcak² · Michael S. Ross³ · Alex Arkowitz¹

Received: 14 August 2019 / Revised: 26 December 2019 / Accepted: 7 January 2020
© Coastal and Estuarine Research Federation 2020

Abstract

High-resolution satellite imaging represents a potentially effective technique to monitor cyclone-caused environmental damage and recovery over large areas at a high spatial scale. This study utilized a 10-m resolution Sentinel satellite image series to document vegetation changes in a portion of the Florida Keys, USA, over which the core of Category 4 Hurricane Irma passed on 10 September 2017. A previously assembled field survey was used to establish land-cover patterns in the satellite data, and concurrent field measurements verified post-hurricane changes. Normalized difference vegetation index (NDVI) was utilized as a tracer for pre-storm baseline patterns and through 19 post-storm months. NDVI patterns show that the severity of vegetation damage varied appreciably across the area, with the least damage on islands in the western sector of the hurricane's eye and around its center, and greatest damage on islands just east of the eye. The data reveal that for 2.5 months after the storm, multiple inland vegetation classes showed substantial early regrowth. However, mangrove forests were more negatively affected. The storm caused extensive mortality of black mangrove (*Avicennia germinans*) and red mangrove (*Rhizophora mangle*), corresponding to more than 40% of the total mangrove area on some islands. The full extent of mangrove die-off was not immediately evident, and increased progressively through the first few months after the storm. In addition to demonstrating the utility of high-resolution satellite image series for post-hurricane environmental assessment, this study reveals high-resolution links between vegetation types, their location within the cyclone, and the extent of post-storm recovery.

Keywords Hurricane Irma · Remote sensing · NDVI · Image series · Mangroves

Introduction

Tropical cyclones are large and intense disturbances known for their vast ecological and economic damage potential. Even within their core path, however, environmental damage tends to be quite variable. This is due to the storms' inherent spatial variability in wind speed and direction, the height and

direction of their storm surge, and their interaction with abiotic and biotic features of the affected land areas. Damage to vegetative cover can be affected by the surrounding topography's influence on wind exposure (Boose et al. 2004) and storm surge (Smith et al. 2009), and soil characteristics, which will affect windthrow (Everham and Brokaw 1996). Biotic factors affecting damage severity include tree species, size (Walker et al. 1991), and stand attributes such as species composition (Craighead and Gilbert 1962; Zimmerman et al. 1994). Another factor—the severity of vegetation damage relative to its position within the hurricane—has not been frequently documented. Wadsworth and Englerth (1959) observed significant damage up to 43 km from the track of the eye of Hurricane Betsy in Puerto Rico and Thompson (1983) observed varying effects of Hurricane Allen in Jamaica up to 60 km from its eye. Hu and Smith (2018) noted a strong relationship with remotely sensed damage parameters for more than 70 km from Hurricane Maria's track in Puerto Rico. The timing of assessment is also important in characterizing hurricane impacts, as many short-term effects of a storm

Communicated by Brian B. Barnes

✉ Jan Svejkovsky
jan@oceani.com

¹ Ocean Imaging Corp., 13976 W, Bowles Ave, Suite 100, Littleton, CO 80127, USA

² Institute of Environment, Florida International University, 11200 SW 8th St, Miami, FL 33199, USA

³ Southeast Environmental Research Center and Department of Earth & Environment Florida, International University, Miami, FL 33199, USA

can disappear rapidly through natural recovery processes (Tanner et al. 1991). Conversely, Smith III et al. (1994) surveyed mangrove areas in the USA's Florida Everglades over several months after Hurricane Andrew and found certain mangrove species and size classes to experience a delayed mortality effect that added 50% to the initial mortality estimates.

Smith et al.'s (1994) observations exemplify that vegetation damage surveys done shortly after the passage of a hurricane do not by themselves provide accurate information about long-term survival and possible recovery. A time series of post-storm comprehensive damage assessment surveys is thus needed to best guide post-hurricane natural resource management. Compared to logistically difficult and often costly field surveys, satellite imaging provides several potential advantages for longer-term monitoring of hurricane vegetation damage and subsequent recovery trends: (1) large regions can be assessed synoptically; (2) spatial measurements can be extracted from the imagery much more easily than during overflight estimates; (3) archived data may be available to establish pre-storm, baseline conditions; and (4) post-storm monitoring can be extended for months or years.

A number of studies have utilized low resolution (1 km and 250 m) and medium resolution (30 m) satellite remote sensing to assess post-hurricane damage to coastal and upland forests (Ramsey et al. 1998; Ayala-Silva and Twumasi 2004; Rodgers et al. 2009; Hu and Smith 2018). Others summarized long-term changes to mangroves due to hurricanes (Han et al. 2018) and chilling events (Zhang et al. 2016), and to model future storm damage to mangroves (Zhang et al. 2019). Such studies faced two important challenges: (1) distinguishing (i.e., classifying) different vegetation types in the multispectral data with sufficient accuracy, and (2) having potentially insufficient spatial resolution to adequately reflect the highly variable landcover distributions and high spatial variability in storm damage. Hu and Smith (2018) minimized the first problem by utilizing relatively broad landcover classifications in their Hurricane Maria-related work in Puerto Rico and Dominica. For example, their "wetland" class included/combined emergent wetland, mudflats, mangrove forests, and *Pterocarpus* swamp. In a different study using a multi-decadal (30 m resolution) satellite image series to monitor changes in Everglades mangrove distributions, Han et al. (2018) used pixel unmixing techniques and comparisons to higher resolution aerial photo data to reduce the second problem—spatial resolution effects.

Attempting to advance from the limitations of earlier hurricane damage-related satellite remote sensing studies, we utilized a relatively high spatial resolution (10 m) satellite multispectral image time series coupled with a previously established, detailed, high resolution landcover field survey and aerial mapping project to monitor temporal changes in multiple vegetation types that experienced the full force of

2017's Hurricane Irma in the Florida Keys, south of USA's Florida mainland. Our objectives were (1) to evaluate the utility of high resolution satellite remote sensing techniques to detect spatial and temporal post-hurricane changes in different land-cover types on plant species and spatial scales that have been previously documented only with field studies or visual aerial surveys, (2) to utilize remote sensing to detect and quantify spatial patterns of vegetation damage severity within the hurricane footprint, and (3) to evaluate the extent of vegetation recovery in the most heavily damaged region through 1.5 years after the storm's passage at spatial resolutions not utilized with previous hurricanes.

Methods

Study Area and the Passage of Hurricane Irma

The Florida Keys are an archipelago of limestone islands extending southwestward from the Florida mainland. The islands support a variety of ecosystems ranging from dwarf mangrove mudflats and fringe mangrove forests to pine rocklands with canopies of slash pine (*Pinus elliottii* var. *densa*) and hardwood hammocks inhabited by tropical tree species whose centers of distribution lie further south. The region's annual cycle is characterized by very distinct wet and dry seasons. The rainy season in the Florida Keys typically runs from June through October, including the majority of the hurricane season, which officially ends on November 30th (NOAA 2019). This cycle is reflected in the seasonal growth of many plant species, whose vigor is reduced during the dry winter and spring months.

The area is regularly subjected to hurricanes that cause damage not only from the wind's physical force but also from storm surges that wash over the islands, and from sediment deposition. Many notable hurricanes have impacted the Keys during the last century (Esri 2019). One was the 1935 "Labor Day hurricane" whose center passed over the upper Keys as a Category 5 storm on the Saffir-Simpson scale, and caused an estimated 5.5–6 m storm surge. Hurricane Donna made landfall in the upper Keys on the morning of 10 September 1960 as a Category 4 storm, and was subsequently regarded as the strongest and most destructive Keys storm until Hurricane Irma in 2017 which also made landfall in the lower Keys the morning of 10 September as a Category 4. Prior to Irma, the most recent hurricane event was Hurricane Wilma in 2005, a Category 3 storm, which passed northwest of the Keys but caused two successive storm surges that inundated the islands (Kasper 2007).

Our study area comprised a series of neighboring islands in the lower Florida Keys that were affected by Hurricane Irma's strongest winds (Ross et al. 2019). These islands were also subject to detailed airborne light detection and ranging

(LiDAR) surveys and the generation of very high resolution land cover classification map products for the US Fish and Wildlife Service in 2006 (Zhang et al. 2010). The resulting land cover maps defined the study area and were used as a base layer for this project's satellite data analysis (see next section). The islands include Big Pine Key, Little Pine Key, No Name Key, Little Torch Key, Middle Torch Key, Big Torch Key, Cudjoe Key, and Sugarloaf Key (Figs. 1 and 3). Also included in this study, but not classified during 2006, were multiple small islands in the vicinity of Big Pine Key that were primarily mangrove-covered.

Hurricane Irma was a long-lived Cape Verde hurricane that made four landfalls across northern Caribbean islands as a Category 5 storm, before crossing the Florida Keys as a Category 4. It made landfall at eastern Cudjoe Key around 9:00 AM local time on 10 September 2017, with maximum sustained winds of 213–222 km/h. Hurricane force winds (sustained winds >118 km/h) extended out up to 130 km from the center. The storm passed over the Keys in a north-northwestward direction at 330°, moving relatively slowly at

13 km/h (Cangialosi et al. 2018). Post-storm surveys indicated that the combined effect of storm surge and tide produced inundation levels 1.5 to 2.5 m above ground level (Cangialosi et al. 2018). This implies that large portions of the largest islands, and all of the smaller, low-lying islands and peninsulas became completely submerged during the hurricane's passage.

Satellite Imagery

Multiple high-resolution multispectral satellite image sources were considered for this study, including the RapidEye, Sentinel, SPOT, and WorldView satellites. Cloud-free image data availability at reasonable time intervals during the initial 6-month post-hurricane period proved to be a limiting factor. The Sentinel satellite constellation provided the highest number of reasonably cloud-free images of the study region during that time frame. The two Sentinel-2 satellites available are part of the EU's Copernicus Programme. These satellites provide multispectral visible-nearIR imagery at 10 m resolution (ESA

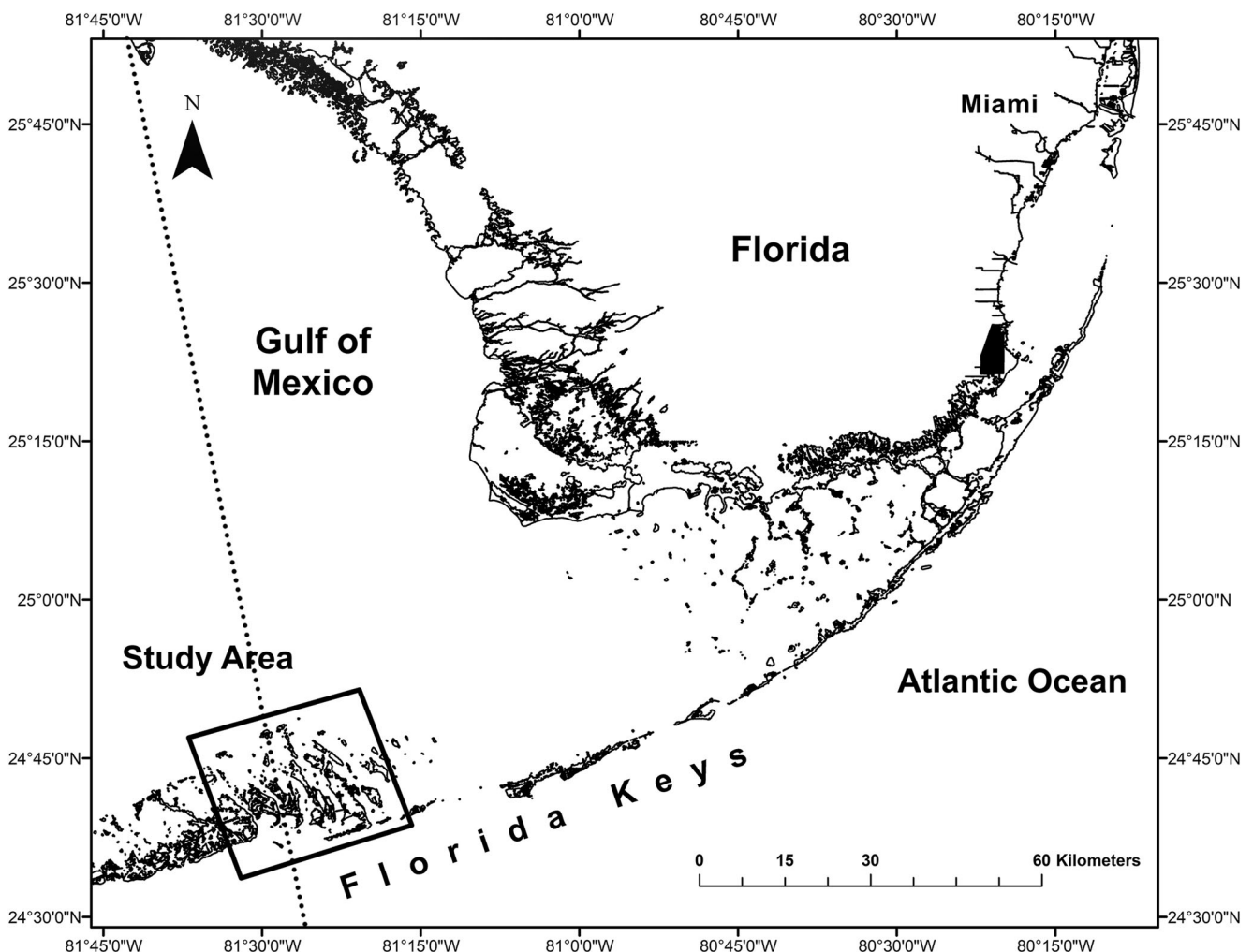


Fig. 1 Location of study area in the lower Florida Keys (USA). Dotted line shows northward path of Hurricane Irma

2019a). This study utilized 13 post-storm images with minimal cloud contamination spanning 3 October 2017 to 1 May 2019. We also used imagery from 1 October 2016, 25 February 2017 and 4 August 2017 (the last relatively cloud-free image available before Hurricane Irma) for pre-storm comparisons (Table 1).

Each image set was electronically retrieved as a NetCDF data package from <https://scihub.copernicus.eu/dhus/#/home>. Data sets acquired after December 2018 were retrieved as Level 2A reflectance products, which include Bottom-of-Atmosphere atmospheric correction and a cloud mask (ESA 2019b). Data sets acquired prior to December 2018 are only available as Level 1C products and were processed to the 2A level using the Sentinel Application Platform (SNAP) and Sen2Cor application software available at <https://step.esa.int/main/third-party-plugins-2/sen2cor/>. To maintain processing consistency, the same parameters were used as applied by ESA in their own post-December 2018 Level 1C product generation. All follow-on image processing was done using ArcMap 10.3.1 software. The Level 2A cloud mask was found inadequate on some of the images, and did not mask cloud shadow areas. Therefore, the cloud masks were manually corrected using heads-up digitizing methods.

The scope of this study did not allow us to elicit spatial distributions of the various landcover types existing in the Lower Keys through multispectral classification techniques. Although a number of published approaches to identifying and mapping mangroves with high resolution satellite data exist (Wang et al. 2005; Vijay et al. 2005; Neukermans et al. 2008; Wan et al. 2018), validated techniques for most of the other landcover types present are lacking. Instead, we utilized

data from an existing published and validated landcover map produced by Florida International University for the US Fish and Wildlife Service (Zhang et al. 2010). The map covers the islands listed in the Study Area section above. The land-cover maps were derived using a combination of LiDAR-based digital elevation data, aerial imagery and extensive field sampling and verifications. The land-cover classification system was adapted from a hierarchical TWINSPAN classification of major Florida Keys' ecosystem types, consisting of 13 ecological site units ranging from tidal wetlands to upland forests (Ross et al. 1992).

Initial first-responder post-storm field and aerial surveys revealed that many areas in the study region experienced significant (and in some cases near-complete) defoliation, making multispectral vegetation index computation a good approach to quantify defoliation severity. Vegetation indices computed from various combinations of channels in multispectral satellite or aerial data have been widely used to assess parameters related to vegetation leaf density and vigor. The most commonly utilized index is the normalized difference vegetation index (NDVI), defined as

$$NDVI = \frac{(NIR - Red)}{(NIR + Red)}$$

where red and NIR are the spectral reflectance measurements acquired in the red (visible) and near-infrared regions, respectively. NDVI is a dimensionless value between -1 and $+1$. Typically, vigorous, dense plant canopies exhibit values above 0.5, shrubs and meadows are in the 0.2–0.3 range, bare soils 0.0–0.1, and clouds, water and snow are 0.0 or negative (Pettorelli 2013). A variation—NDWI which substitutes the near-IR band with a short wave-IR band (Gao 1996) - was found to work well for detecting cold stress in mangroves (Zhang et al. 2016), and NDVI has been successfully used to assess hurricane damage to vegetation in previous studies (Rodgers et al. 2009; Steyer et al. 2013; Hu and Smith 2018). Since NDVI has a strong documented correlation to leaf area index (Carlson and Ripley 1997; Wang et al. 2005), we deemed it as the most direct tracer of large changes in leaf density across the various Irma-impacted vegetation classes. With the Sentinel data, Bands 4 (664.6 nm center, 31 nm bandwidth) and 8 (832.8 nm center, 100 nm bandwidth) were used for the Red and near-IR components, respectively. To trace changes in NDVI in time, NDVI differences ($\Delta NDVI$) were also computed between NDVI image pairs. In some cases this required re-rectifications of portions of an image (using road intersections and other obvious tie-points) to eliminate slight spatial differences between the images before subtraction.

Polygons for each type of landcover class from the Zhang et al. (2010) digital GIS maps were used to isolate the corresponding areas in the NDVI and $\Delta NDVI$

Table 1 Satellite imagery used in this study

Date	Satellite	Time (UTC)	Sun elevation (°)
10/1/2016	Sentinel 2A	T 16:00:52	56.57
2/25/2017	Sentinel 2A	T16:05:11	48.92
8/4/2017	Sentinel 2A	T16:05:11	68.49
9/10/2017	Hurricane Irma		
10/3/2017	Sentinel 2A	T16:05:11	56.6
11/25/2017	Sentinel 2A	T16:06:11	41.71
1/4/2018	Sentinel 2A	T16:06:41	38.45
2/23/2018	Sentinel 2A	T16:04:09	48.64
3/22/2018	Sentinel 2A	T16:05:11	58.18
4/21/2018	Sentinel 2A	T16:05:11	67.44
7/25/2018	Sentinel 2B	T16:05:08	69.28
10/21/2018	Sentinel 2A	T16:09:35	51.57
12/7/2018	Sentinel 2A	T16:05:03	39.59
1/11/2019	Sentinel 2B	T16:05:10	38.88
1/21/2019	Sentinel 2B	T16:05:11	40.23
2/28/2019	Sentinel 2A	T16:02:11	49.94

image products. For the analysis of spatial variation in post-storm vegetation damage, all polygons of each vegetation class on each mapped island were utilized to compute the 1 October 2016–3 October 2017 Δ NDVI. Pixels that were cloud contaminated in either image were masked before the subtraction, then the Δ NDVI mean was computed from each island's available pixels for each vegetation class. Middle Torch and Little Torch Keys contained too much cloud contamination to be included in the analysis. No Name Key, one of the most storm-affected keys and one in which most landcover categories were represented, was chosen for the long-term recovery analysis of the five most prevalent landcover classes. Representative polygon subsections from Zhang et al.'s (2010) database were utilized, and their locations and extents are shown in Fig. 2c.

Field Data

Field sampling surveys were conducted throughout October–November 2017 and January 2018, targeting areas of interest identified from the imagery. Field surveys that included low-level drone color photography were conducted in January 2019 and additional field surveys were done in April 2019. Multiple mangrove mortality surveys were done at four sites in the Long Beach peninsula area beginning in November 2017. A portion of a mangrove polygon was identified at each study site on the satellite images, based on initial field recognition. In the field a 12 × 15 m sample area was then marked off from the edge of the polygon inward using GPS and marking tape attached to corner trees. During November 2017, January 2018, January 2019, and April 2019 surveys, all trees

in the sample plot were counted and classified as “alive” or “dead”. Criteria for the “dead” designation were as follows: no leaves on branches, and thoroughly cracked/peeling, dry bark on the stem. At each site, two shallow soil samples were extracted by coring with a 2-cm PVC pipe to a depth of 20 cm during the November 2017 survey. Cores were extruded and the depth of storm sediment deposit was measured to the nearest millimeter.

Results

Initial Post-Storm Vegetation Damage Assessment

Pre-hurricane (1 October 2016) “baseline” NDVI distribution patterns in the study region show that most of the islands were covered with vigorous vegetation exhibiting NDVI values greater than 0.5, which is generally interpreted as high leaf density and chlorophyll content (Birky 2001; Lüdeke et al. 1991) (Fig. 3a). Exceptions were bare soil areas (with NDVI values near 0.0) primarily located in urbanized zones, and submerged and exposed mudflat areas with NDVI values at 0 or slightly negative. Some of those areas contained living dwarf mangroves, but at densities too low, at 10 m pixel resolution, to appreciably elevate the NDVI values.

The seasonally corresponding post-storm NDVI result from 3 October 2017 – the first mostly cloud-free post-storm Sentinel image acquired 23 days after Irma's passage – presents a different picture, in which the overall NDVI values are significantly reduced, corresponding to the combined effects of partial defoliation and physical damage to tree and shrub limbs and stems (Fig. 3b). Areas containing “hardwood

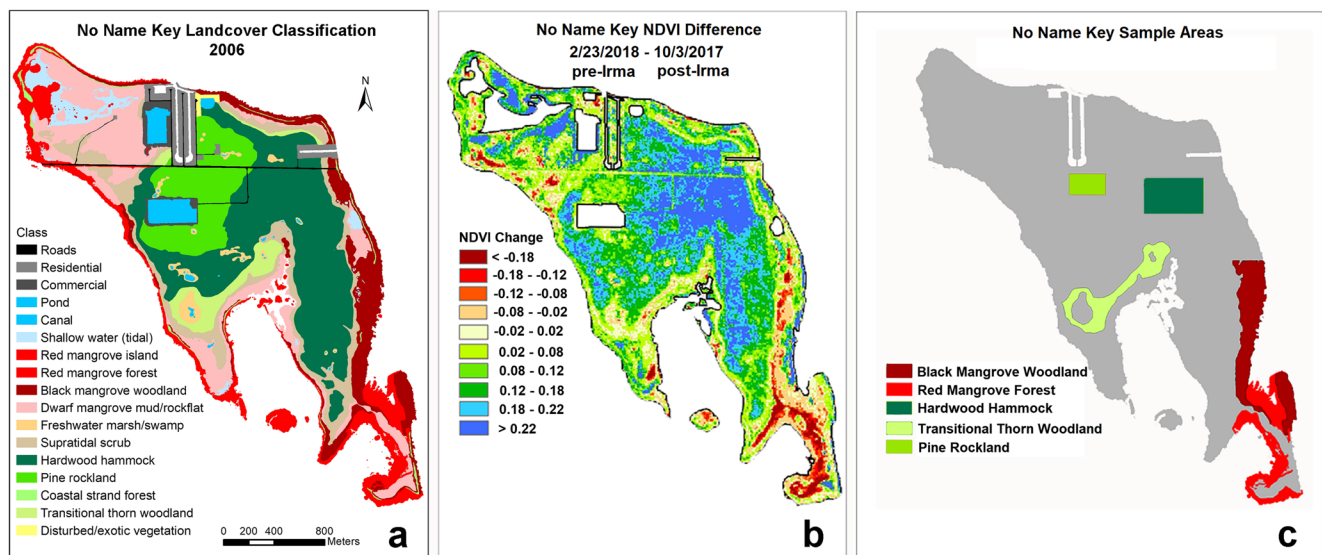
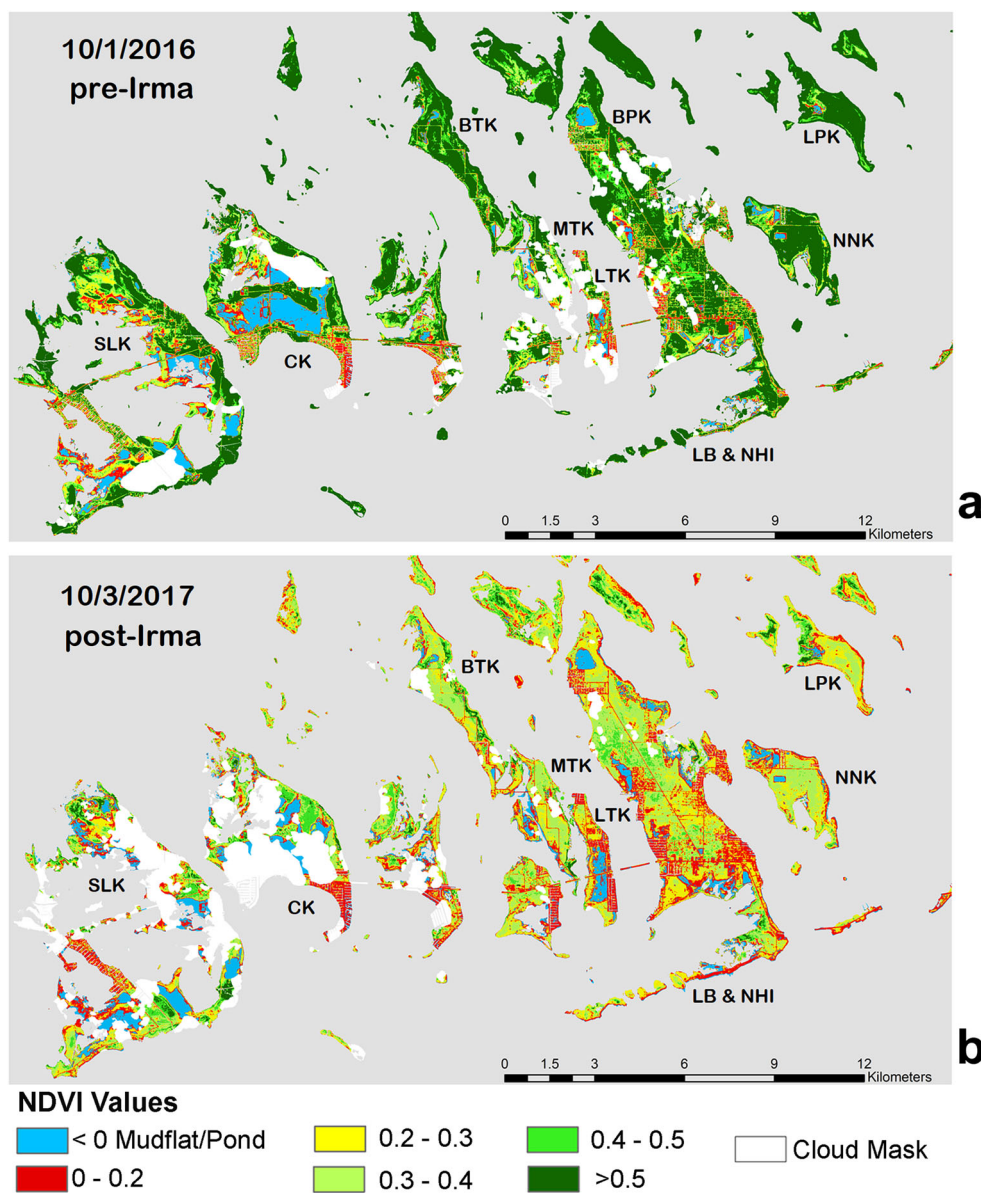


Fig. 2 **a** No Name Key landcover classification from Zhang et al. (2010) and **b** post-Irma NDVI change from 10/3/2017 to 2/23/2018, showing close correspondence between different vegetation communities and their

different regrowth responses. **c** Locations of polygon sections used to trace NDVI changes from 10/1/2016 (11 months pre-Irma) to 5/1/2019 (19 months post-Irma)

Fig. 3 NDVI maps from pre-Irma 10/1/2016 (a), and post-Irma 10/3/2017 (b). SLK = Sugarloaf Key, CK = Cudjoe Key, BTK = Big Torch Key, MTK = Middle Torch Key, LTK = Little Torch Key, BPK = Big Pine Key, NNK = No Name Key, LPK = Little Pine Key, LB&NHI = Long Beach Peninsula and Newfound Harbor Islands



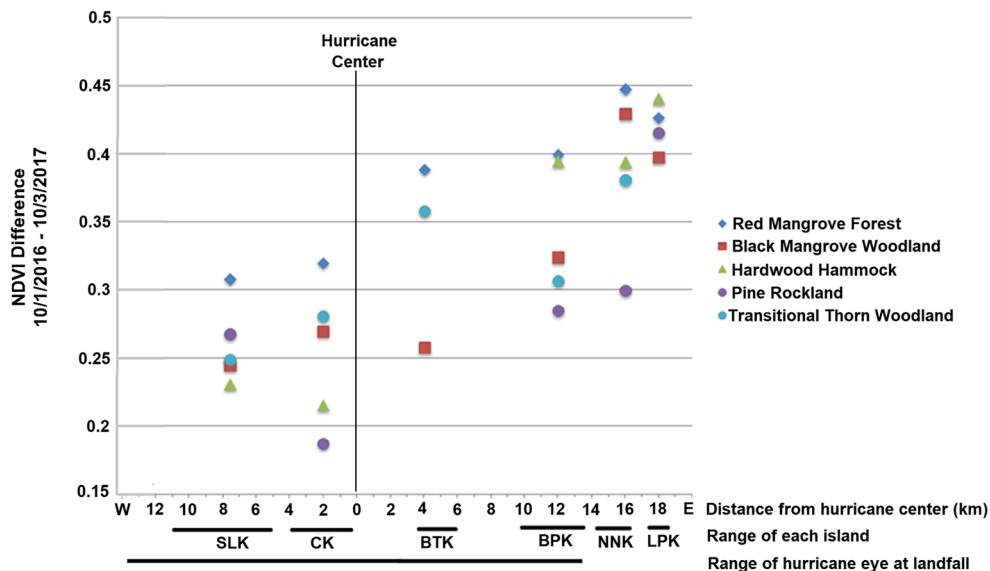
hammock,” “pine rockland,” and mangrove landcover classes show NDVI broad-scale decreases of 30–50+ % compared to October 2016 values. Urbanized zones show a drastic NDVI reduction from their much broader pre-Irma range to values approaching zero.

To assess spatial patterns in the initial vegetation damage, we computed the mean Δ NDVI for each island between the 1 October 2016 and 3 October 2017 images for several major landcover classes: red mangrove (*Rhizophora mangle*), black mangrove (*Avicennia germinans*), hardwood hammock, pine rockland, and transitional thorn woodland. The data are presented in Fig. 4 relative to distance from the center of hurricane Irma’s eye at landfall on eastern Cudjoe Key. There is a clear east-west trend, indicating less damage for all classes on islands west of and around the epicenter of the hurricane

eye. As judged by the NDVI decrease, the greatest damage was experienced on No Name and Little Pine Keys—the two easternmost islands that were just east of the hurricane eye, and thus experienced persistent eyewall winds.

For mangrove areas, the NDVI decrease from the 2016 baseline was approximately 30% greater on No Name and Little Pine Keys compared to Sugarloaf and Cudjoe Keys. A similar east-west trend was observed for the hardwood hammock class, with a 45% larger decrease on the easternmost islands. The eastward and southeastward-facing shores of both of the easternmost islands (as well as the Long Beach/Newfound Harbor Islands region) also exhibited bands 100–250 m wide of 0 and near-zero NDVI values on 3 October 2017 (visible in Fig. 3b). Most but not all of these features correspond to red and black mangrove areas that were completely defoliated and suffered extreme physical damage.

Fig. 4 Mean NDVI land cover type differences between images acquired on 10/1/2016 (pre-Irma) and 10/3/2017 (post-Irma) on each island. The islands' position is shown relative to east-west distance from Irma's eye center at landfall. (Eye position and extent were measured from archived KAMX-Miami radar imagery.) Island name coding is the same as in Fig. 3



Post-Storm Recovery Trends

NDVI changes in the months following Irma's passage differed among vegetation classes. This is exemplified in a Δ NDVI image of No Name Key—one of the most affected islands—shown in Fig. 2b. The Δ NDVI patterns closely match Zhang et al.'s (2010) main vegetation class polygons (Fig. 2a).

We utilized polygon subsections of the main vegetation classes on No Name Key to follow the post-storm recovery through the following 19 months, using NDVI as a tracer. Results are shown in Fig. 5. The greatest positive changes correspond to the hardwood hammock area, as was also observed on other islands. The results indicate that this forest lost 76% of its NDVI-indicated leaf density between pre-storm (4 August 2017) and earliest post-storm (3 October 2017)

images. It then vigorously refoliated, and by 25 November 2017 (76 days after the storm), it exhibited 94% of its pre-storm NDVI value. The transitional thorn woodland and pine rockland classes responded similarly, though with lesser intensity. The pine rockland class presents a problem for accurate NDVI change interpretation, because the slash pines present are rarely dense enough to form a continuous upper canopy. Instead, even with 10 m resolution imagery, each pixel value represents an integration of reflectances from the pines and underlying vegetation, commonly thatch palms (*Leucothrinax morrisii*), poisonwood trees (*Metopium toxiferum*) and numerous shrubs and grasses. The pines suffered severe initial physical damage and delayed mortality, likely related to salinization of soil and groundwater associated with the storm surge (Ross et al. 2019; Kiflai et al. 2019). However, by the time of this project's November 2017 field

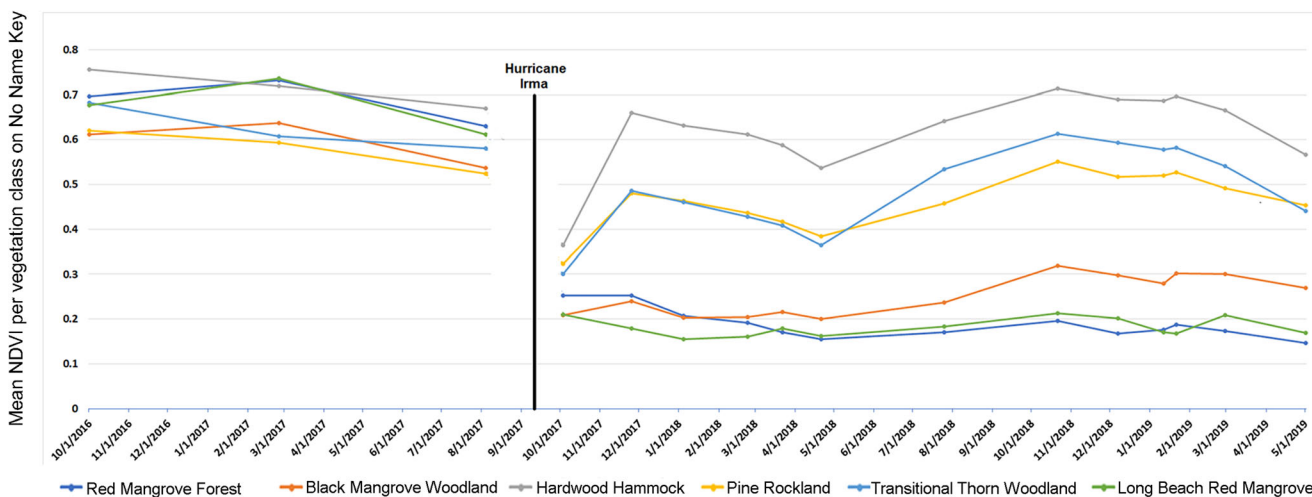


Fig. 5 Mean NDVI values for different vegetation class sample areas on No Name Key shown in Fig. 2. in cloud-free imagery between 10/1/2016 (11 months pre-Irma) and 5/1/2019 (19 months post-Irma)

work, the thatch palms and poisonwood in most pine rocklands had already extended new leaves. It is thus very likely that the positive NDVI change recorded in the pine rockland areas in the October to November 2017 interval was due to associated taxa, not the pines themselves.

The initial refoliation and regrowth for the non-mangrove classes occurred during the first 3 months following the storm and ceased by the end of November 2017. This corresponded to the onset of the Keys' dry season which was quite severe in 2017–2018. Frequent seasonal rains resumed in late April, 2018, corresponding to a multi-month increase in NDVI which peaked in the 21 October 2018 image. All three non-mangrove vegetation classes show higher NDVI peaks than following the previous year's post-storm refoliation, although none reached levels measured in October 2016, prior to the hurricane.

Mangrove Mortality

Imagery from our No Name Key time series indicates that black and red mangrove areas experienced the sharpest declines in plant vigor over the 19-month post-Irma period (Fig. 5). This was also observed on other islands, exemplified by Site 2 on the Long Beach peninsula, also included in Fig. 5. The decline was not immediate, however. Some mangrove areas still had partial green leaf coverage for several months after the storm. This was field-verified in multiple locations at the time. Black mangroves, in particular, exhibited epicormic growth into November 2017 (possibly seen as a November rise in the No Name Key data). As the NDVI series in Fig. 5 reveals, however, the mangrove areas continued to decline through January and February, 2018. Field surveys of several of the highest die-off zones in January 2018 showed 90+ % mortality, with no correlation to tree size or mangrove species. Field sampling was used to determine that an NDVI value of 0.2 or less corresponds to a zone filled with standing or fallen bare stems and branches, dead organic matter on the ground and, by January 2018, 90+ % tree mortality. Using Zhang et al.'s (2010) landcover classification polygons for red and black mangroves, areas exhibiting NDVI values ≤ 0.2 in imagery from 23 February 2018 represented 46% of total pre-storm mangrove cover on No Name Key, 42% on the Long Beach peninsula/Newfound Harbor Islands, and 21% on Little Pine Key.

The four 90+ % mortality sites in the Long Beach/Newfound Harbor region designated for more detailed study are inland of the fringe mangrove zone and receive minimal tidal flushing. Soil core samples taken during the November 2017 surveys showed a surface layer of carbonate mud ranging from 1.2–3.2 cm thick ($n = 8$), which also adhered to the trees' prop roots and pneumatophores. Site 4 was dominated by black mangrove, with the others containing primarily red mangrove.

Figure 6 shows the locations and 90% + mortality status (≤ 0.2 NDVI) of sites on Long Beach peninsula on 2/23/2018, as well as low altitude drone images acquired on 1/3/2019. The drone images document the continued lack of appreciable regrowth 15 months after the hurricane. Based on NDVI changes between 23 February 2018 and 28 February 2019, site 2 maintained its 90+ % mortality state, and sites 1 and 4 indicated slight regrowth. Site 3 reverted to well above the 90% threshold in the 28 February 2019 satellite image data. Field observations done in April 2019 revealed that while Site 1 then contained a few sparse patches of live saplings, the increase in satellite-derived NDVI values at site 4 and particularly at site 3 was due to colonization of the areas by the herbaceous halophytes, *Batis maritima* and *Salicornia ambigua*, but with no evidence of actual mangrove recovery. Similarly, the black mangrove forest site on No Name Key where a 59% NDVI increase occurred between May and October 2018 (Fig. 5) was due to herbaceous halophyte encroachment, not mangrove regrowth.

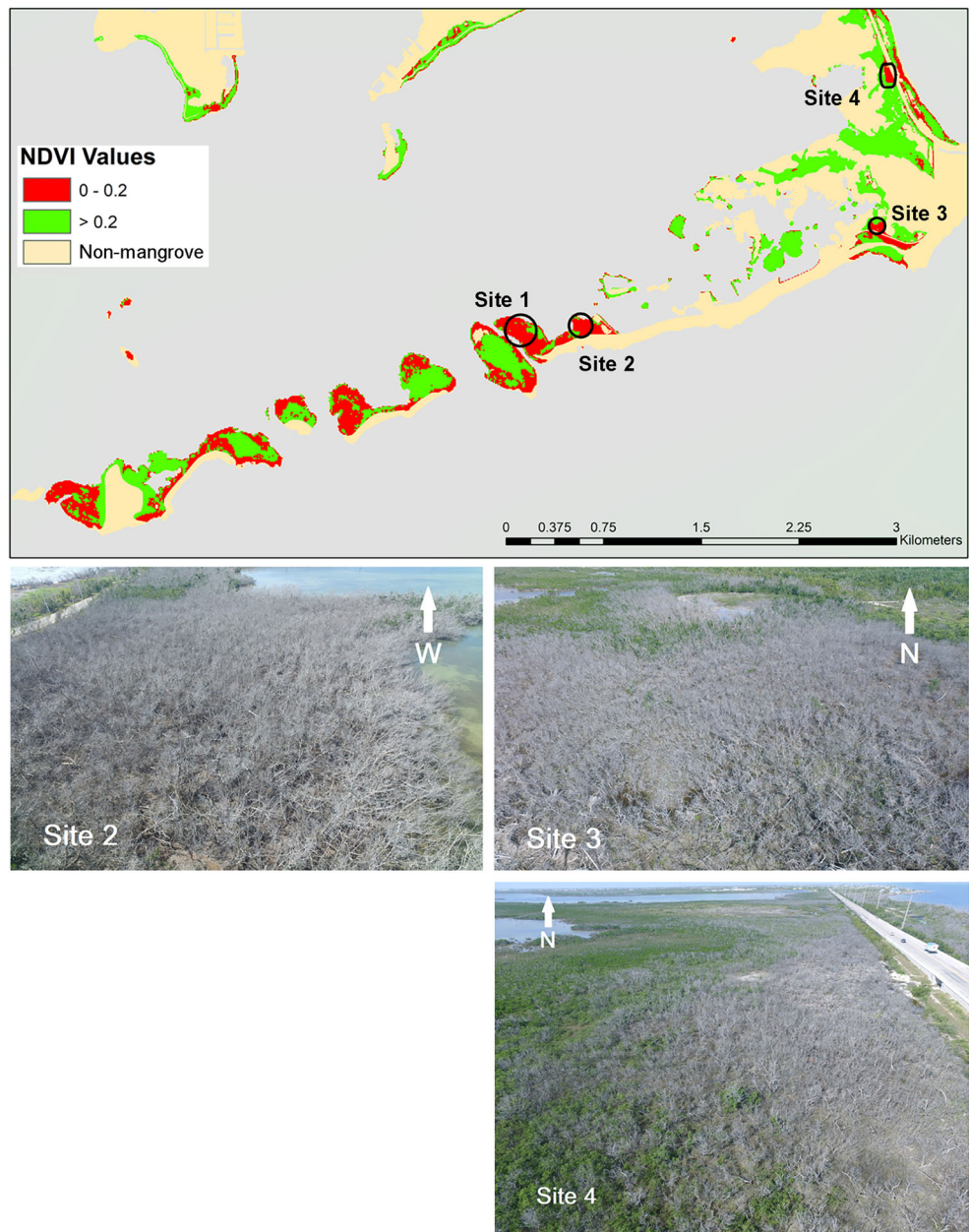
Discussion

Our results demonstrate that high-resolution multispectral satellite imagery can be used effectively to not only observe immediate changes in vegetation conditions after a hurricane, but also to monitor longer term post-storm trends using simple indicator indices such as the NDVI. The large footprint, synoptic monitoring capability of multi-satellite constellations such as Sentinel-2 provide relatively frequent revisit times, thereby increasing the likelihood of having sufficiently cloud-free imagery available at an acceptable temporal frequency. With 10 m spatial resolution and adequate ground-truthing, post-storm monitoring can be done on a plant community or even individual species level (in the case of mangroves).

The results show that high-resolution satellite image series acquired through the post-hurricane months can document several vegetation response patterns at spatial scales previously reported using only field and aerial visual surveys. The post-Irma satellite observations of extreme defoliation in hardwood hammock species (as judged by large NDVI decreases) followed by rapid regrowth within the first 2–3 months concur with field and aerial observations after Hurricanes Donna (Craighead and Gilbert 1962) and Andrew (Smith et al. 1994) in the Florida Everglades.

The short-term non-mangrove vegetation recovery observations indicate rapid regrowth took place during the 2nd and 3rd months after the storm's passage, but no usable Sentinel imagery was available during the first 3 weeks post-storm to assess when the recovery began. Hu and Smith's (2018) NDVI-based observations of short-term vegetation recovery in Puerto Rico and Dominica after Hurricane Maria included

Fig. 6 NDVI values of mangrove forest areas in the Long Beach Rd. and Newfound Harbor Islands region on 2/23/2018 showing locations of field observation sites, and corresponding drone photos acquired on 1/3/2019. (Site 1 can only be reached by boat and was not accessed on 1/3/2019.)



imagery acquired 2 days after its landfall in Dominica as well as a month later. They concluded that there was little recovery after 1 month but significant recovery after 1.5 months. The timeline of their regrowth observations thus corresponds very closely to this study's results in the Florida Keys.

Tanner et al. (1991) note that massive defoliation creates enormous input of litter to the soil, and results in a pulse of available mineral nutrients. In Puerto Rico's subtropical forests, soil nitrification increased for 7 months following Hurricane Hugo (Tanner et al. 1991), and relatively fast refoliation was also observed there. This study's Florida Keys observations of rapid refoliation of hardwood hammock, transitional thorn woodland, and pine rockland during the 2nd

through 3rd months following the storm fall within the nutrient increase timeline. It is not known, however, whether the increased nutrient availability indeed helped fuel the observed regrowth in either location. Our results indicate that complete recovery (as judged by the NDVI values) was not reached for any of the non-mangrove classes within the post-storm 19 months covered in this study, although hardwood hammock came close. Ogurcak (2015) studied the response of hardwood hammock and pine rockland in the same area of the Florida Keys following Hurricanes Georges (1998) and Wilma (2005). Utilizing vegetation indices computed from a long time series of medium resolution (30 m) satellite imagery, she found it took 3 years for hardwood hammock areas to

reach pre-storm index values, and more than 6 years for the pine rocklands to do so.

This study also demonstrates that coincident field sampling is necessary to properly link the high resolution satellite-observed changes to the plant species responsible, since species dominance may have shifted significantly from pre-hurricane distributions. This is exemplified by findings that NDVI increases in the pine rocklands were due to species other than pines, and increases in NDVI in black mangrove forest were attributable to colonization of the understory by other halophytes, rather than to recovery by mangroves. It is likely that full return to pre-hurricane leaf area will require recovery in the dominant canopy species as well as in understory associates.

NDVI patterns derived from the first cloud-free post-Irma image on 3 October 2017 revealed the relation between initial vegetation damage severity and position within the hurricane core. The strongest winds within northern hemisphere hurricanes occur in the right-side eyewall relative to the storm's forward motion (NOAA 2014)—i.e., the eastern side in the case of Hurricane Irma. Based on the NDVI differences between western and eastern islands, mangrove trees and hammock species in the eastern eyewall likely suffered 30–45% greater defoliation within a distance of merely 16–18 km.

The Sentinel satellite NDVI image series allowed tracking of the recovery of several vegetation classes through an entire wet/dry season annual cycle. As noted above, a very strong regrowth spurt of non-mangrove vegetation types was observed shortly after the storm, peaking at greater than 80% recovery of pre-storm NDVI values by late November—the start of the annual dry season. Additional recovery was observed in the NDVI series during the following year's wet season, a time of year when even the evergreen mangroves exhibit increased leaf area (Zhang et al. 2016). Hence, the timing of hurricanes like Irma in regions with distinctive dry and wet seasons may influence the extent of the initial recovery: late-season storms may result in a shorter first year recovery window than early season storms which are followed by several months of optimal growing conditions.

The satellite data also documented severe Irma-caused damage to mangroves, paralleling Craighead and Gilbert's (1962) observations following Hurricane Donna, and delayed additional mangrove mortality noted by Smith et al. (1994) after Hurricane Andrew. Smith et al. (1994) reported that although damaged and severely defoliated, many red mangroves continued to bear some green leaves a month after the storm, and black mangroves and white mangroves (*Laguncularia racemosa*) were observed resprouting new growth. Subsequent surveys indicated, however, that they eventually succumbed to hurricane damage. Our data series from No Name Key indicate onset of a continued decline approximately 2 months after the storm. The post-hurricane delayed mangrove mortality phenomenon was most recently

reported by Radabaugh et al. (2019), whose continued post-Irma field work includes study plots in the Florida Keys 5 to 15 km west of this project's study region. Based on the strong east-west Δ NDVI post-storm gradient revealed in this study (Fig. 4), their study sites likely experienced only a fraction of mangrove defoliation that occurred on islands some 30–40 km to the east. They estimate initial (2 months post-storm) mortality at 19%, which then increased to 36% through the following 7 months. None of their study sites suffered the extensive mortalities that the satellite data recorded further to the east. This study revealed isolated areas which at 4 months post-storm exhibited 90+ % mangrove mortality. While many of these dead zones were located in the hardest-hit eastern half of the study area, they were also observed irregularly in the western half, particularly along the Atlantic-facing shoreline of Sugarloaf Key. On the hardest-hit islands, they represent a loss of 20–40+ % of the total pre-Irma mangrove forest coverage.

Radabaugh et al.'s (2019) work links the delayed mortality of both black and red mangroves to the thickness of the storm-deposited carbonate mud layer. Black mangroves can die if their pneumatophores are partially or fully covered by sediment (Lee et al. 1996; Ellison 1998). Lenticels (breathing pores) of red mangroves are primarily located just above the soil level on their prop roots and the trees can asphyxiate if these are buried by excess sediment (Terrados et al. 1997; Ellison 1998). Our field observations in several of the satellite-located 90+ % die-off zones showed relatively high sediment accumulations not only as a ground layer but also as hard accretions on the roots themselves. The near-total mortality zones that were field-surveyed were basin-type forests with minimal tidal flushing, some only reached by periodic peak tides. Additionally, during the extremely dry weather that began in November 2017, little rain was available to facilitate washing off the accreted sediment. We therefore propose that in addition to the initial extensive physical damage, anoxia due to the accumulated sediment may have followed, contributing to the formation of the near-total mortality zones.

An obvious question is how (or if) such areas will repopulate with mangroves. Those that comprise the inshore extent of a fringe mangrove zone (e.g., sites 1 and 2 in this study) can be envisioned to repopulate progressively with mangroves from the shoreline inward as tides and currents bring new propagules into the dead zone, and the newly established plants then provide future seed stock for the interior. Other areas that are fully cut-off from regular tidal flow (e.g., sites 3 and 4) may take a long time to repopulate, if at all. In their long-term study of Everglades mangrove response to several hurricanes, Han et al. (2018) found that most areas recovered within 3 to 4 years after a major hurricane, but some smaller areas did not recover at all.

The concept of replanting such areas has been recently raised by volunteer groups in the Florida Keys. Mangrove

forest restoration has historically experienced mixed success, with the “Ecological Mangrove Restoration” (EMR) process (Lewis 2009) being the best documented and most widely implemented approach. EMR stresses biophysical assessments and eco-hydrological repair over mass replanting, which has relevance to the Florida Keys situation. It is unclear at present if the soil conditions in the highest mortality areas have improved enough to sustain new plantings. In addition to the unflushed silt, other soil conditions such as increased sulfide levels (Smith et al. 1994) could continue to make such areas inhospitable to the plantings. These areas of high tree mortality are also at risk of peat collapse which occurs when continued compaction and decomposition of dead organic matter is not offset by new root growth (Cahoon et al. 2003, Barr et al. 2012.) This can result in a loss of surface elevation and a conversion of the original mangrove habitat to mud flats (Smith et al. 2009; Barr et al. 2012), especially along coastlines that are experiencing very high rates of sea-level rise, such as those in South Florida (Wdowinski et al. 2016). High resolution satellite imaging can provide a convenient aid for future field monitoring linked to any potential remediation efforts.

Acknowledgments The satellite processing/analysis and field sampling work on this project were funded by Ocean Imaging Corporation. We thank Collin Forbes for the drone photography work. We also thank Chris Bergh from The Nature Conservancy for coordinating this project's team. This is contribution number 941 from the Southeast Environmental Research Center in the Institute of Environment at Florida International University.

References

- Ayala-Silva, T., and Y.A. Twumasi. 2004. Hurricane Georges and vegetation change in Puerto Rico using AVHRR satellite data. *International Journal of Remote Sensing* 25 (9): 1629–1640.
- Barr, J.G., V. Engel, T.J. Smith, and J.D. Fuentes. 2012. Hurricane disturbance and recovery of energy balance, CO₂ fluxes and canopy structure in a mangrove forest of the Florida Everglades. *Agricultural and Forest Meteorology* 153: 54–66.
- Birky, Alicia K. 2001. NDVI and a simple model of deciduous forest seasonal dynamics. *Ecological Modeling* 143: 43–58.
- Boose, E.R., M.I. Serrano, and D.R. Foster. 2004. Landscape and regional impacts of hurricanes in Puerto Rico. *Ecological Monographs* 74 (2): 335–352.
- Cahoon, D.R., P. Hensel, J. Rybczyk, K.L. McKee, C.E. Proffitt, and B.C. Perez. 2003. Mass tree mortality leads to mangrove peat collapse at Bay Islands, Honduras after hurricane Mitch. *Journal of Ecology* 91 (6): 1093–1105.
- Cangialosi, J.P., A.S. Latta, and R. Berg. 2018. *National Hurricane Center Tropical Cyclone Report, Hurricane Irma*. NOAA 22pp.
- Carlson, T.N., and D.A. Ripley. 1997. On the relation between NDVI, fractional vegetation cover and leaf area index. *Remote Sensing of Environment* 62: 241–252.
- Craighead, F.C., and V.C. Gilbert. 1962. The effects of Hurricane Donna on the vegetation of southern Florida. *Quarterly Journal Florida Academy of Sciences* 25: 1–28.
- Ellison, J.C. 1998. Impacts of sediment burial on mangroves. *Marine Pollution Bulletin* 37 (8–12): 420–426.
- ESA. 2019a. Sentinel-2 User Handbook. https://sentinel.esa.int/documents/247904/685211/Sentinel-2_User_Handbook. Accessed 9 August 2019.
- ESA. 2019b. Sentinel User Guides. <https://sentinel.esa.int/web/sentinel/user-guides/sentinel-2-msi/processing-levels/level-2>. Accessed 6 October 2019.
- Esri. 2019. The 15 worst hurricanes in Florida Keys history. <https://www.arcgis.com/apps/MapSeries/index.html?appid=795c97208a234a22be68f487854478c5>. Accessed 17 December 2019.
- Everham, E.M., III, and N.V.L. Brokaw. 1996. Forest damage and recovery from catastrophic wind. *Botanical Review* 62: 113–185.
- Gao, B.C. 1996. NDWI – A normalized difference water index for remote sensing of vegetation liquid water from space. *Remote Sensing of Environment* 58: 257–266.
- Han, X., L. Feng, C. Hu, and P. Kramer. 2018. Hurricane-induced changes in Everglades National Park mangrove forest: Landsat observations between 1985 and 2017. *Journal of Geophysical Research: Biogeosciences* 123: 3470–3488.
- Hu, T., and R.B. Smith. 2018. The impact of Hurricane Maria on the vegetation of Dominica and Puerto Rico using multispectral remote sensing. *Remote Sensing* 10 (6): 827.
- Kasper, K. 2007. *Hurricane Wilma in the Florida keys*. NOAA <https://www.weather.gov/key/wilma>. Accessed 9 August 2019.
- Kiflai, M.E., D. Whitman, D.E. Ogurcak, and M. Ross. 2019. The effect of Hurricane Irma storm surge on the freshwater lens in Big Pine Key, Florida using electrical resistivity tomography. *Estuaries and Coasts*: 1–13. <https://doi.org/10.1007/s12237-019-00666-3>.
- Lee, S.K., W.H. Tan, and S. Havanond. 1996. Regeneration and colonization of mangrove on clay-filled reclaimed land in Singapore. *Hydrobiologia* 319 (1): 23–35.
- Lewis, R.R. 2009. Methods and criteria for successful mangrove forest restoration. In *Coastal Wetlands: An Integrated Ecosystem Approach*, ed. G.M.E. Perillo, E. Wolanski, D.R. Cahoon, and M.M. Brinson, 787–800. Elsevier Press.
- Lüdeke, M., A. Janecek, and G.H. Kohlmaier. 1991. Modelling the seasonal CO₂ uptake by land vegetation using the global vegetation index. *Tellus* 43B: 188–196.
- Neukermans, G., F. Dahdouh-Guebas, J.G. Kairo, and N. Koedam. 2008. Mangrove species and stand mapping in Gazi Bay (Kenya) using Quickbird satellite imagery. *Spatial Science* 53 (1): 75–84.
- NOAA. 2014. <https://www.aoml.noaa.gov/hrd/tcfaq/D6.html>. Accessed 9 August 2019.
- NOAA. 2019. Florida Keys Climate Data. <https://www.weather.gov/key/climate>. Accessed 9 August 2019.
- Ogurcak, D. E. 2015. The effect of disturbance and freshwater availability on lower Florida keys' coastal Forest dynamics. FIU Electronic Theses and Dissertations. 2288. <https://digitalcommons.fiu.edu/etd/2288>
- Pettorelli, N. 2013. *The normalized difference vegetation index*. Oxford Press 213pp.
- Radabaugh, K.R., R.P. Moyer, A.R. Chappel, E.E. Dontis, C.E. Russo, K.M. Joyse, M.W. Bownik, A.H. Goekner, and N.S. Khan. 2019. Mangrove damage, delayed mortality, and early recovery following hurricane Irma at two landfall sites in Southwest Florida, USA. *Estuaries and Coasts*.
- Ramsey, E.W., D.K. Chappell, D.M. Jacobs, S.K. Sapkota, and D.G. Baldwin. 1998. Resource management of forested wetlands: Hurricane impact and recovery mapped by combining Landsat TM and NOAA AVHRR data. *Photogrammetric Engineering and Remote Sensing* 64 (7): 733–738.
- Rodgers, J., A. Murrach, and W. Cooke. 2009. The impact of Hurricane Katrina on the coastal vegetation of the Weeks Bay Reserve, Alabama from NDVI data. *Estuaries and Coasts* 32: 496–507.

- Ross, M.S., J.J. O'Brien, and L.J. Flynn. 1992. Ecological site classification of Florida Keys terrestrial habitats. *Biotropica* 24: 488–502.
- Ross, M.S., D.E. Ogurcak, S. Stoffella, J.P. Sah, J. Hernandez, and H. Willoughby. 2019. Hurricane Irma and the structural decline of pine forests on a low Florida Keys island. *Estuaries and Coasts*: 1–13. <https://doi.org/10.1007/s12237-019-00624-z>.
- Smith, T.J., III, M.B. Robblee, H.R. Wanless, and T.W. Doyle. 1994. Mangroves, hurricanes, and lightning strikes. *BioScience* 44: 256–262.
- Smith, T.J., III, G.H. Anderson, K. Balentine, G. Tiling, G.A. Ward, and K.R. Whelan. 2009. Cumulative impacts of hurricanes on Florida mangrove ecosystems: Sediment deposition, storm surges and vegetation. *Wetlands* 29 (1): 24–34.
- Steyer, G.D., B.R. Couvillion, and J.A. Barras. 2013. Monitoring vegetation response to episodic disturbance events by using multitemporal vegetation indices. *Journal of Coastal Research* 63: 118–130.
- Tanner, E.V.J., V. Kapos, and J.R. Healey. 1991. Hurricane effects on forest ecosystems in the Caribbean. *Biotropica* 23 (4a): 513–521.
- Terrados, J., U. Thampanya, N. Srichai, P. Kheowvongsri, O. GeertzHansen, S. Boromthananarath, N. Panapitukkul, and C.M. Duarte. 1997. The effect of increased sediment accretion on the survival and growth of *Rhizophora* apiculate seedlings. *Estuarine, Coastal and Shelf Science* 45 (5): 697–701.
- Thompson, D.A. 1983. Effects of Hurricane Allen on some Jamaican forests. *Commonwealth Forestry Review* 62: 107–115.
- Vijay, V., R. S. Biradar, A. B. Inamdar, G. Deshmukhe, S. Baji, and M. Pikle. 2005. Mangrove mapping and change detection around Mumbai (Bombay) using remotely sensed data. *Indian Journal of Marine Sciences* 34 (3): 310–315.
- Wadsworth, F.H., and G.H. Englerth. 1959. Effects of the 1956 hurricane on forests in Puerto Rico. *Caribbean Forester* 20: 38–51.
- Walker, L.R., D.J. Lodge, N.V.L. Brokaw, and R.B. Waide. 1991. An introduction to hurricanes in the Caribbean. *Biotropica* 23: 313–331.
- Wan, L., H. Zhang, T. Wang, and H. Lin. 2018. Mangrove species discrimination from very high resolution imagery using Gaussian Markov random field model. *Wetlands* 38 (5): 861–874.
- Wang, Q., S. Adiku, J. Tenhunen, and A. Granier. 2005. On the relationship of NDVI with leaf area index in a deciduous forest site. *Remote Sensing of Environment* 94: 244–255.
- Wdowski, S., R. Bray, B.P. Kirtman, and Z. Wu. 2016. Increasing flooding hazard in coastal communities due to rising sea level: Case study of Miami Beach, Florida. *Ocean & Coastal Management* 126: 1–8.
- Zhang, K., M. Ross, D. Ogurcak, and P. Houle. 2010. Lower Florida Keys digital terrain model and vegetation analysis for the National Key Deer Refuge. Final report. US Fish and Wildlife Service.
- Zhang, K., B. Thapa, M. Ross, and D. Gann. 2016. Remote sensing of seasonal changes and disturbances in mangrove forest: A case study from South Florida. *Ecosphere* 7 (6): 1–23.
- Zhang, C., S.D. Durgan, and D. Lagomasino. 2019. Modeling risk of mangroves to tropical cyclones: A case study for hurricane Irma. *Estuarine, Coastal and Shelf Science* 224: 108–116.
- Zimmerman, J.K., E.M. Everham III, R.B. Waide, D.J. Lodge, C.M. Taylor, and N.V.L. Brokaw. 1994. Responses of tree species to hurricane winds in subtropical wet forest in Puerto Rico: Implications for tropical tree life histories. *Journal of Ecology* 82: 911–922.